PHYSICAL REVIEW B **89**, 020505(R) (2014)

Noncentrosymmetric superconductor with a bulk three-dimensional Dirac cone gapped by strong spin-orbit coupling

Mazhar N. Ali,[1,*] Quinn D. Gibson,[1] T. Klimczuk,[2,3] and R. J. Cava[1,†]

[1]*Department of Chemistry, Princeton University, Princeton New Jersey, 08544, USA*

[2]*Faculty of Applied Physics and Mathematics, Gdansk University of Technology, Narutowicza 11/12, 80-233 Gdansk, Poland*

[3]*Institute of Physics, Pomeranian University, Arciszewskiego, 76-200 Slupsk, Poland*

(Received 30 October 2013; revised manuscript received 27 December 2013; published 14 January 2014)

The layered, noncentrosymmetric heavy element $PbTaSe_2$ is found to be superconducting. We report its electronic properties accompanied by electronic-structure calculations. Specific heat, electrical resistivity, and magnetic-susceptibility measurements indicate that $PbTaSe_2$ is a moderately coupled, type-II BCS superconductor ($T_c = 3.72$ K, Ginzburg–Landau parameter $\kappa = 17$) with an electron-phonon coupling constant of $\lambda_{ep} = 0.74$. Electronic-structure calculations reveal a single bulk three-dimensional Dirac cone at the K point of the Brillouin zone derived exclusively from its hexagonal Pb layer; it is similar to the feature found in graphene except there is a 0.8 eV gap opened by spin-orbit coupling. The combination of large spin-orbit coupling and lack of inversion symmetry also results in large Rashba splitting on the order of tenths of an eV.

DOI: 10.1103/PhysRevB.89.020505 PACS number(s): 74.70.Xa, 74.20.Pq

Noncentrosymmetric superconductors have been known for decades but have become a prominent research topic recently with the discovery of the heavy-fermion superconductor $CePt_3Si$ [1]. Noncentrosymmetric systems can exhibit asymmetric spin-orbit coupling (SOC) in superconducting materials, which leads to the breaking of spin degeneracy and a parity-mixed superconducting state [2]. The symmetry of the Cooper pairs is therefore nontrivially affected by the strength of the SOC, which is governed by the crystal structure as well as the elemental composition [3,4]. Superconductors that lack inversion symmetry can be divided into two types: strongly correlated systems such as $CePt_3Si$ [1] and UIr [5], and weakly correlated systems such as Li_2M_3B (M = Pd, Pt) [6,7] and $Mg_{10}Ir_{19}B_{16}$ [8]. In the strongly correlated materials, the superconducting properties are heavily influenced by the electron correlations making the weakly correlated materials more fertile ground for studying the effects derived from the breaking of inversion symmetry and the asymmetric spin-orbit-coupling interaction. Materials with strong SOC are also of interest as exotic spin systems [9] and topological insulators [10,11] (TIs), and relativistic Dirac electrons in condensed-matter systems are of interest on the surface of TIs, in graphene and other monatomic hexagonal lattices [12–15], and also in the bulk of three-dimensional (3D) Dirac semimetals (e.g., Cd_3As_2, Na_3Bi, and $Pb_{1-x}Sn_xSe$ [16–19]). Recent theoretical work has predicted SOC gapping in Dirac cones at the K point in crystallographic phases similar to, but heavier than, graphene [20]. Here we show that the hexagonal, noncentrosymmetric compound $PbTaSe_2$ exhibits strong SOC, superconducts below 3.72 K and has a gapped graphene-like Dirac cone at K in its electronic structure that is derived exclusively from its hexagonal Pb layer.

$PbTaSe_2$ displays alternating stacking of hexagonal $TaSe_2$ and Pb layers [21]. The crystal structure is highly noncentrosymmetric as can be seen by inspecting the Ta positions in the inset of Fig. 1(a). High-quality polycrystalline samples were synthesized by solid-state reaction at 800 °C for one week using prereacted PbSe, $TaSe_2$, and elemental Ta powder in sealed quartz tubes in a PbSe atmosphere. The samples were determined to be pure by powder x-ray diffraction. Due to the polycrystalline nature of the samples, the measured superconductivity parameters are averaged over all crystallographic directions.

The superconducting transition was examined through temperature-dependence measurements of the electrical resistivity $\rho(T)$ and dc magnetic susceptibility using a Quantum Design physical property measurement system (PPMS). The whole temperature range of $\rho(T)$ is shown in Fig. 1(a). The normal-state resistivity for $PbTaSe_2$ reveals a metallic-like character ($d\rho/dT > 0$), with the residual resistivity ratio RRR ≈6. The superconducting transition is seen just below 3.8 K. Figure 1(b) shows the superconducting transition characterized by dc magnetic susceptibility. The much smaller field-cooling (FC) signal compared with the zero-field-cooling (ZFC) signal is caused by pinning of the vortices. The estimated superconducting critical temperature, as determined by the midpoints of the transitions, is 3.7 K, in agreement with resistivity measurements. The diamagnetic response, normalized by a demagnetization factor, is very close to the expected value. Figure 1(c) shows the low-temperature resistivity $\rho(T)$ under zero field and applied magnetic fields up to 0.5 T. A very sharp superconducting transition is observed for 0 T, with the superconducting critical temperature $T_c = 3.79$ K and transition width $\Delta T_c = 0.15$ K. Knowing the values of T_c for different magnetic fields, we plot the upper critical field values, $\mu_0 H_{c2}$ vs temperature in Fig. 1(d). The upward curvature of the upper critical field line may be due to an intrinsically anomalous pairing mechanism. The previously proposed formula [22] $H_{c2}(T) = H_{c2}(0)(1 - t^{3/2})^{3/2}$, where $t = \frac{T}{T_c}$ was used to fit the whole $H_{c2}(T)$ data set and gives an excellent fit ($R^2 = 0.999\,96$) with $\mu_0 H_{c2}(0) = 1.47$ T [Fig. 1(d), solid blue line]. This model has been used to fit $H_{c2}(T)$ for noncentrosymmetric $Nb_{0.18}Re_{0.82}$ [23] and the borocarbide superconductors [24]. Alternatively, the orbital critical field, for a single-band, BCS-type superconductor, is given by $H_{c2}(T) = -AT_c \frac{dH_{c2}}{dT}|_{(T=T_c)}$ where A is either 0.69

*mnali@princeton.edu
†rcava@princeton.edu

 ©2014 American Physical Society

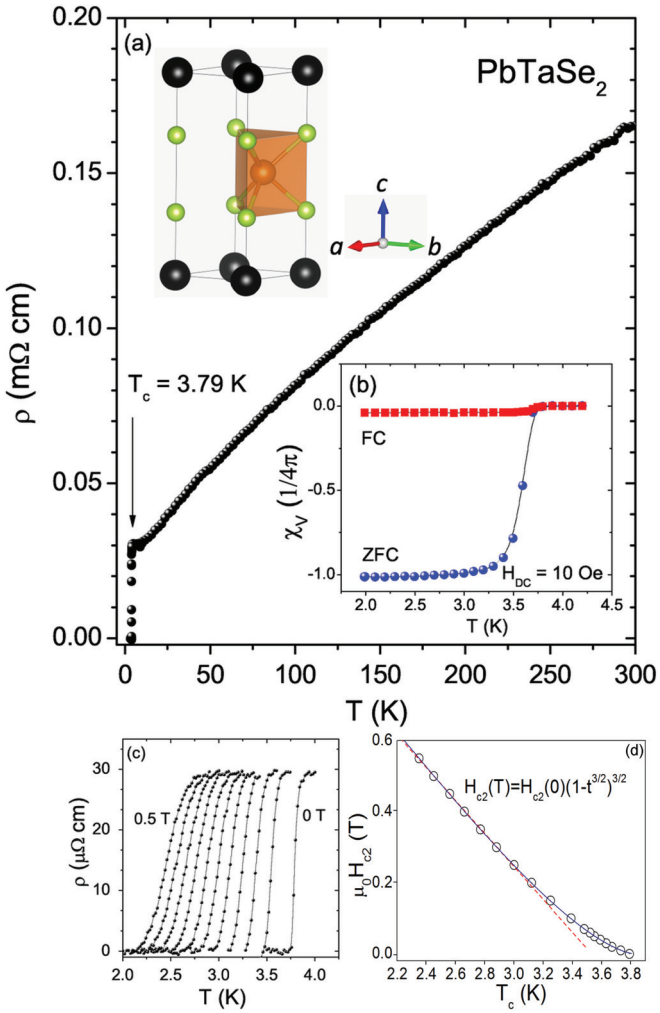

FIG. 1. (Color online) (a) Resistivity as a function of temperature showing the superconducting transition for $PbTaSe_2$ at 3.79 K. Inset: The crystal structure of $PbTaSe_2$, where Pb are the large black spheres, Se are the small green spheres, and Ta are the medium orange spheres. (b) The observed zero-field-cooling (ZFC) and field-cooling (FC) magnetic-susceptibility measurements under magnetic field $H_{DC} =$ 10 Oe. The superconducting critical temperature T_c estimated from these measurements is 3.72 K. The maximum ZFC susceptibility is estimated to be $-1.01(1/4\pi)$. (c) The superconducting transition under various magnetic fields and (d) plots of the upper critical field values vs temperature. The red dashed line through the data shows the best linear fit with the slope $dH_{c2}/dT = -0.46$ T/K. The solid blue line shows the fit to equation shown with $R^2 = 0.999\,96$.

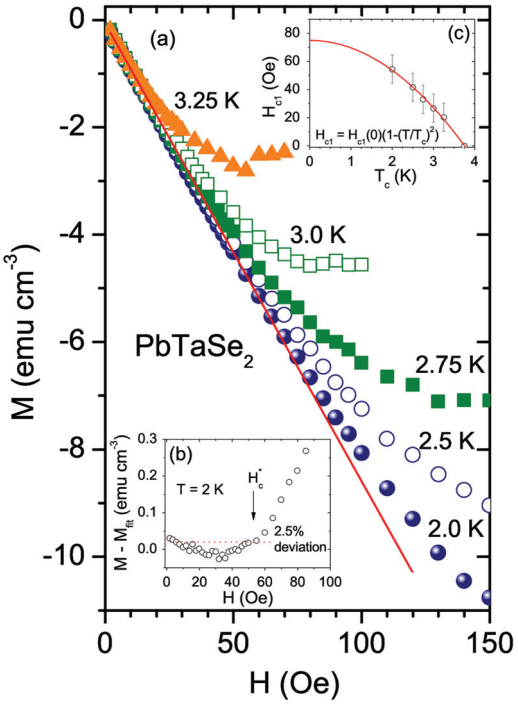

FIG. 2. (Color online) (a) M vs H for $PbTaSe_2$ at various temperatures. The solid red line is fit to the 2 K data in the low-H range where the linear $M(H)$ is observed. (b) The difference between magnetization measured at 2 K and the $M_{\rm fit}$: the difference $M(H) - M_{\rm fit}$ deviates more than 2.5% above the fitted curve for $H_c^* \approx 53$ Oe. (c) The estimation of $\mu_0 H_{c1}(0)$ done by fitting the H_{c1} data to the formula $H_{c1}(T) = H_{c1}(0)[1 - (T/T_c)^2]$, which is represented by the red solid line.

or 0.73, for the dirty or clean limits, respectively [25]. From Fig. 1(d), the slope $dH_{c2}/dT = -0.46$ T/K was determined for the temperature range 2.3 K $< T <$ 3 K (dashed red line) and, taking $T_c = 3.72$ K, the orbital upper critical field was estimated as $\mu_0 H_{c2} = 1.18$ T or 1.25 T for the dirty or clean limit, respectively, both of which are close to that obtained by the more detailed fitting procedure. For further calculations we employ $\mu_0 H_{c2}(0) = 1.47$ T. With this information, the coherence length can be calculated by using the Ginzburg–Landau formula $\xi_{GL}(0) = \{\phi_0/[2\pi H_{c2}(0)]\}^{1/2}$, where $\phi_0 = h/2e$ and is found to be $\xi_{GL}(0) = 15$ nm.

Assuming that the initial linear response to field is perfectly diamagnetic [Fig. 2(a)], i.e., dM/dH is $-\frac{1}{4\pi}$, we obtain a demagnetization factor that is consistent with the sample shape and its orientation in the magnetic field. Figure 2(a) shows the magnetization (M) as a function of applied field (H) and Fig. 2(b) presents the difference between magnetization measured at 2 K and the $M_{\rm fit}$ [shown as a red solid line in Fig. 2(a)] fit in the low-H range where the linear $M(H)$ is observed. As shown in Fig. 2(b), $M(H)$ starts to deviate from $M_{\rm fit}$ at a field H_c^* of about 53 Oe, giving a lower critical field, taking into account the demagnetization factor, of $H_{c1}(2K) = H_c^*/(1-d) = 60$ Oe. The estimation of $\mu_0 H_{c1}(0)$ has been done by fitting experimental data to the formula $H_{c1}(T) = H_{c1}(0)[1 - (T/T_c)^2]$, which is represented by the red solid line in Fig. 2(c). The estimated zero-temperature lower critical field $\mu_0 H_{c1}(0) = 7.5$ mT implies a Ginzburg–Landau superconducting penetration depth calculated using

$$\mu_0 H_{c1} = \frac{\Phi_0}{4\pi\lambda_{GL}^2} \ln \frac{\lambda_{GL}}{\xi_{GL}}$$

of approximately $\lambda_{GL} = 248$ nm. The Ginzburg–Landau parameter $[\kappa = \lambda_{GL}(0)/\xi_{GL}(0)]$ is $\kappa = 17$, indicating that $PbTaSe_2$ is a type-II superconductor. Using these parameters and the relation $H_{c1}H_{c2} = H_c^2 \ln(\kappa)$, we estimated the thermodynamic critical field $\mu_0 H_c = 57.4$ mT.

The heat capacity was measured using a relaxation calorimeter (Quantum Design PPMS). Figure 3(a) illustrates

MOST WIEDZY Downloaded from mostwiedzy.pl

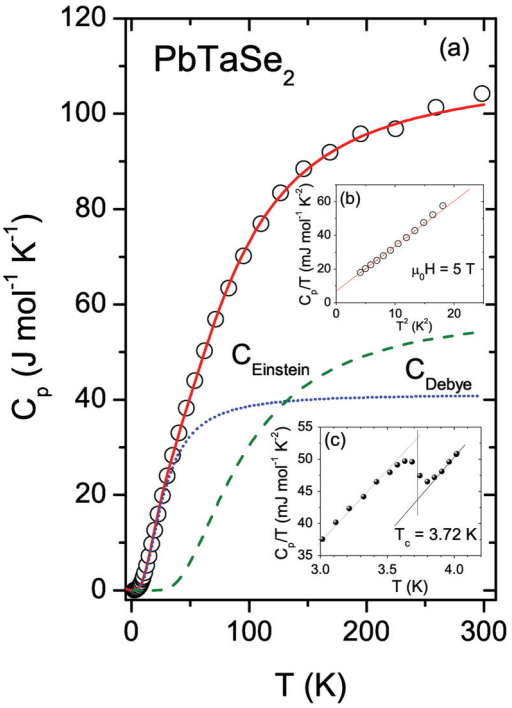

FIG. 3. (Color online) (a) The specific heat versus temperature measurements represented by the open circles. The solid red line is a fit to a combined model where 41% of the weight is given to the Debye model (dotted blue line) and 59% to the Einstein model (dashed green line). (b) C_p/T versus T^2 with the red line showing the linear fit in the low-temperature region. (c) C_p/T versus T showing the bulk superconducting jump and the equal-area approximation for the T_c determination.

the overall temperature dependence of the specific heat C_p. At room temperature, C_p is close to the expected Dulong–Petit value ($3nR \approx 100$ J mol^{-1} K^{-1}), where n is the number of atoms per formula unit ($n = 4$), and R is the gas constant ($R = 8.314$ J mol^{-1} K^{-1}). Figure 3(b) shows C_p/T versus T^2 in the low-temperature range measured under a magnetic field of $\mu_0 H = 5$ T, which exceeds the upper critical field for $PbTaSe_2$. The experimental data points were fit in the temperature range of 1.9 K to 3.7 K by using the formula $C_p = \gamma T + \beta T^3$. The fit yields the electronic specific-heat coefficient (Sommerfeld coefficient) $\gamma = 6.9\,(2)$ mJ mol^{-1} K^{-2}, and phonon specific-heat coefficient $\beta = 2.67\,(0.03)$ mJ mol^{-1} K^{-4}. Bulk superconductivity is confirmed by a large anomaly [Fig. 3(c)] at a $T_c = 3.72$ K as determined by the entropy-balance method. This is consistent with T_c determined by the dc magnetic-susceptibility and resistivity measurements. Using γ and the specific-heat-jump value $\Delta C/T_c$ at the superconducting transition temperature, $\Delta C/\gamma T_c$ can be calculated and is found to be 1.41, which is very close to the BCS value of 1.426.

In a simple Debye model, the β coefficient is related to the Debye temperature (Θ_D) through $\Theta_D = (\frac{12\pi^4}{5\beta} nR)^{\frac{1}{3}}$, and the estimated Debye temperature for $PbTaSe_2$ is only 143 K, which reflects the fact that it contains heavy elements. As can be seen from Fig. 3(a), C_{Debye} with $\Theta_D = 143$ K (dotted blue line) is not large enough to reach the experimental heat-capacity values above 40 K. Therefore we fit the data in the temperature range 10 to 300 K by using the formula $C_p = \gamma T + kC_{\text{Debye}}(T) + (1-k)C_{\text{Einstein}}(T)$, in which higher-energy optical modes are considered. The first term (γT) is the electronic contribution and the k parameter corresponds to the weight of the phonon contributions to the specific heat given by the Debye (C_{Debye}) and Einstein (C_{Einstein}) models, respectively:

$$C_{\text{Debeye}}(T) = 9nR\left(\frac{T}{\Theta_D}\right)^3 \int \frac{x^4 \exp(x)}{[\exp(x-1)]^2},$$

$$C_{\text{Einstein}}(T) = 3nR\left(\frac{\Theta_E}{T}\right)^2 \exp\left(\frac{\Theta_E}{T}\right)\left[\exp\left(\frac{\Theta_E}{T} - 1\right)\right]^{-2}.$$

Θ_D and Θ_E are the Debye and Einstein temperatures, respectively. The fit represented by the solid, red line in Fig. 3(a) gives 41% of the weight to a Debye term with $\Theta_D = 112$ K, close to the temperature derived from the low-temperature fit, and the remaining weight (59%) in an Einstein mode with energy $\Theta_E = 290$ K.

With these results and assuming $\mu^* = 0.13$, the electron-phonon coupling constant λ_{ep} can be calculated from the inverted McMillans formula [26]

$$\lambda_{ep} = \frac{1.04 + \mu^* \ln\left(\frac{\Theta_D}{1.45T_c}\right)}{(1-0.62)\mu^* \ln\left(\frac{\Theta_D}{1.45T_c}\right) - 1.04}$$

and is found to be 0.74. This value is similar to that found in other moderately coupled superconductors such as YPd_2Sn and $HfPd_2Al$ [27]. Having the Sommerfeld parameter and the electron-phonon coupling, the noninteracting density of states at the Fermi energy can be calculated from

$$N(E_F) = \frac{3\gamma}{\pi^2 k_B^2 (1+\lambda_{ep})}.$$

The value obtained for $PbTaSe_2$, $N(E_F) = 1.7$ states eV^{-1} per formula unit, agrees well with the 1.5 states eV^{-1} per formula unit calculated from theoretical predictions (see below). Table 1 compares the measured and derived superconductivity parameters of $PbTaSe_2$ with other noncentrosymmetric superconductors: $Mg_{10}Ir_{19}B_{16}$ and $Nb_{0.18}Re_{0.82}$.

Electronic-structure calculations were performed in the framework of density functional theory using the WIEN2K code [28] with a full-potential linearized augmented plane-wave and local orbitals basis together with the Perdew–Burke–Ernzerhof parametrization of the generalized gradient

TABLE I. Superconducting parameters of $PbTaSe_2$.

Parameter	Unit	$Nb_{0.18}Re_{0.82}$ [23]	$Mg_{10}Ir_{19}B_{16}$ [8]	$PbTaSe_2$
T_c	K	8.8	4.45	3.72
$\mu_0 H_{c1}(0)$	mT	5.57	3.0	7.5
$\mu_0 H_{c2}(0)$	T	17.3	0.77	1.47
$\xi_{GL}(0)$	nm	4.4	21	15
$\lambda_{GL}(0)$	nm	363	404	248
$\kappa(0)$		83	20	17
$\gamma(0)$	mJ mol^{-1} K^{-2}	53.4	52.6	6.9
$\Delta C/\gamma T_c$		1.86	1.60	1.41
$\mu_0 H^{\text{Pauli}}$	T	16.8	8.2	6.8
Θ_D	K	383	280	112
λ_{ep}		0.73	0.66	0.74

MOST WIEDZY Downloaded from mostwiedzy.pl

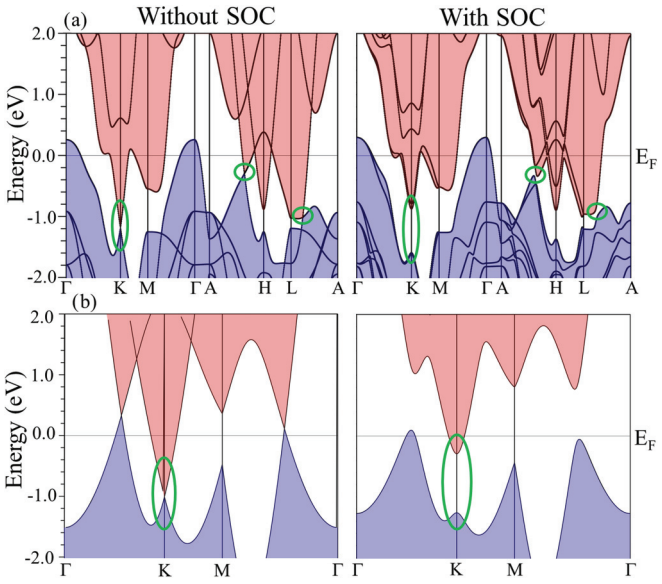

FIG. 4. (Color online) (a) Calculated electronic structures of $PbTaSe_2$ with and without spin-orbit coupling (SOC). Bands are shaded to highlight the continuous gap opened when SOC is included. The Dirac cone that is gapped with SOC as well as band crossings along A-H and A-L, which are similarly gapped implying a possible band inversion, are circled in green. (b) Electronic structure of the two-dimensional Pb sublattice alone in $PbTaSe_2$, with green circles highlighting the Dirac cone that is gapped by SOC at K, just as in bulk $PbTaSe_2$.

approximation [29,30]. In order to check the robustness of the electronic-structure calculations, they were also performed using the Trans–Blaha modified Becke–Johnson (mBJ) functional [31], which resulted in no significant differences.

Band structure calculations for $PbTaSe_2$ immediately unveil a single bulk 3D Dirac cone at the K point in the Brillouin zone that is gapped by large SOC [Fig. 4(a)]. The Dirac cone at K in graphene is also gapped by SOC, albeit by only a few mK; in $PbTaSe_2$, the strong SOC gaps the cone by about 0.8 eV. This single Dirac cone that is gapped by SOC is highly suggestive of $PbTaSe_2$ being topologically nontrivial, as this motif is observed in both graphene [32] (which is a quantum spin Hall insulator) and $Bi_{14}Rh_3I_9$ [33] (which is predicted to be a weak topological insulator). Also, 3D Dirac cones have recently been observed in the two semimetals Cd_3As_2 and Na_3Bi which, if gapped, would drive the systems into the topological insulator regime. Furthermore, the four states that were degenerate at the Dirac point without SOC, when SOC is included, now have different eigenvalues under S6 (C6-bar), C3, and mirror operations. The existence of these symmetries at points where there are possible band inversions suggests the possibility of topological surface states protected by crystalline symmetry, as is seen in topological crystalline insulators [34–36]. Furthermore, although $PbTaSe_2$ is a metal, there is a continuous gap formed around E_F when SOC is considered. A closer look at the electronic structure in Fig. 4(a) reveals two band crossings along A-L and A-H (that are not present along Γ-M or Γ-K, demonstrating that the coupling in the z direction is important) that become gapped with the inclusion of SOC.

The combination of large SOC and broken inversion symmetry is also apparent in the large spin splitting observed in the electronic structure. This is most readily observed around the H point in Fig. 4(a). This spin splitting is on a similar magnitude (in the tenths of eVs) as in the giant Rashba semiconductor BiTeI [37]. In fact, Rashba-type spin splitting is observed around the M and L points around the continuous gap shown in Fig. 4(a). Finally, Fig. 4(b) shows the electronic structure of the Pb sublattice alone. This demonstrates that the Dirac cone observed at K is uniquely due to the Pb sublattice and, with SOC considered, becomes gapped as well. In fact, the Pb sublattice goes from being metallic to being almost completely gapped with the inclusion of SOC. The electronic structure therefore shows that some of the charge carriers in $PbTaSe_2$ are massive 3D Dirac electrons. If the apparent band inversion of the 3D massive Dirac electrons [38] gives rise to a topological crystalline insulator-like state as in $Pb_{0.77}Sn_{0.23}Se$ [34], then a cleaved 001 surface of $PbTaSe_2$ may host Majorana zero modes at the surface even if the bulk superconducting gap is nontrivial, due to the fact that the 001 surface maintains the mirror and C3 symmetries [39]. Furthermore, the large spin splitting observed in the electronic structure indicates the likelihood of an unconventional pairing mechanism that could lead to a nontrivial superconducting gap—another possible way of supporting Majorana fermions at a cleaved surface of $PbTaSe_2$.

In conclusion, we report the discovery of superconductivity in $PbTaSe_2$ and its unusual electronic structure. The single-layer Pb sublattice in $PbTaSe_2$ behaves similarly to graphene monolayers in that it also generates a Dirac point at K, generating 3D massive Dirac fermions by large SOC. Unlike graphene superlattices, however, the inclusion of Pb layers in a natural superlattice with $TaSe_2$ does not affect the in-plane orbitals of Pb that make the Dirac cone at K. This represents a unique case where a two-dimensional (2D) elemental sublattice capable of generating 2D massive Dirac fermions can be interfaced with a transition metal dichalcogenide to create a superconducting superlattice, generating 3D massive Dirac fermions and broken inversion symmetry, all in a thermodynamically stable material. In addition to $PbTaSe_2$ ($T_c = 3.72$ K) and $InTaS_2$ ($T_c \approx 1.0$ K [40]), layered materials of this type [21,41] may represent a new family of materials where the interplay of noncentrosymmetric superconductivity and large SOC can lead to nontrivial electronic topologies.

This research was supported by the US Department of Energy, Grant No. DE FG02-98-ER45706.

[1] E. Bauer, G. Hilscher, H. Michor, C. Paul, E. W. Scheidt, A. Gribanov, Y. Seropegin, H. Noël, M. Sigrist, and P. Rogl, Phys. Rev. Lett. **92**, 027003 (2004).

[2] E. Bauer and M. Sigrist, *Non-Centrosymmetric Superconductors: Introduction and Overview* (Springer, Berlin, 2012), Vol. 847.

MOST WIEDZY Downloaded from mostwiedzy.pl

[3] K. Matano, S. Maeda, H. Sawaoka, Y. Muro, T. Takabatake, B. Joshi, S. Ramakrishnan, K. Kawashima, J. Akimitsu, and G. Zheng, J. Phys. Soc. Jpn. **82**, 084711 (2013).
[4] M. S. Bahramy, R. Arita, and N. Nagaosa, Phys. Rev. B **84**, 041202 (2011).
[5] T. Akazawa, H. Hidaka, T. Fujiwara, T. Kobayashi, E. Yamamoto, Y. Haga, R. Settai, and Y. Ōnuki, J. Phys.: Condens. Matter **16**, L29 (2004).
[6] K. Togano, P. Badica, Y. Nakamori, S. Orimo, H. Takeya, and K. Hirata, Phys. Rev. Lett. **93**, 247004 (2004).
[7] P. Badica, T. Kondo, and K. Togano, J. Phys. Soc. Jpn. **74**, 1014 (2005).
[8] T. Klimczuk, F. Ronning, V. Sidorov, R. J. Cava, and J. D. Thompson, Phys. Rev. Lett. **99**, 257004 (2007).
[9] Y. Okamoto, M. Nohara, H. Aruga-Katori, and H. Takagi, Phys. Rev. Lett. **99**, 137207 (2007).
[10] M. Z. Hasan and C. L. Kane, Rev. Mod. Phys. **82**, 3045 (2010).
[11] H. Zhang, C.-X. Liu, X.-L. Qi, X. Dai, Z. Fang, and S.-C. Zhang, Nat. Phys. **5**, 438 (2009).
[12] K. S. Novoselov, A. K. Geim, S. Morozov, D. Jiang, Y. Zhang, S. Dubonos, I. Grigorieva, and A. Firsov, Science **306**, 666 (2004).
[13] K. Novoselov, A. K. Geim, S. Morozov, D. Jiang, M. K. I. Grigorieva, S. Dubonos, and A. Firsov, Nature (London) **438**, 197 (2005).
[14] A. K. Geim and K. S. Novoselov, Nat. Mater. **6**, 183 (2007).
[15] B. Yan, L. Müchler, and C. Felser, Phys. Rev. Lett. **109**, 116406 (2012).
[16] S. Borisenko, Q. Gibson, D. Evtushinsky, V. Zabolotnyy, B. Buechner, and R. J. Cava, arXiv:1309.7978.
[17] M. Neupane, S. Xu, R. Sankar, N. Alidoust, G. Bian, C. Liu, I. Belopolski, T.-R. Chang, H.-T. Jeng, H. Lin *et al.*, arXiv:1309.7892.
[18] Z. Liu, B. Zhou, Z. Wang, H. Weng, D. Prabhakaran, S.-K. Mo, Y. Zhang, Z. Shen, Z. Fang, X. Dai *et al.*, arXiv:1310.0391.
[19] T. Liang, Q. Gibson, J. Xiong, M. Hirschberger, S. P. Koduvayur, R. Cava, and N. Ong, Nat. Commun. **4**, 2696 (2013).
[20] C.-C. Liu, W. Feng, and Y. Yao, Phys. Rev. Lett. **107**, 076802 (2011).
[21] R. Eppinga and G. Wiegers, Physica B + C (Amsterdam) **99**, 121 (1980).
[22] R. Micnas, J. Ranninger, and S. Robaszkiewicz, Rev. Mod. Phys. **62**, 113 (1990).
[23] A. B. Karki, Y. M. Xiong, N. Haldolaarachchige, S. Stadler, I. Vekhter, P. W. Adams, D. P. Young, W. A. Phelan, and J. Y. Chan, Phys. Rev. B **83**, 144525 (2011).
[24] M. D. Lan, J. C. Chang, K. T. Lu, C. Y. Lee, H. Y. Shih, and G. Y. Jeng, IEEE Trans. Appl. Supercond. **11**, 3607 (2001).
[25] N. Werthamer, E. Helfand, and P. Hohenberg, Phys. Rev. **147**, 295 (1966).
[26] W. McMillan, Phys. Rev. **167**, 331 (1968).
[27] T. Klimczuk, C. Wang, K. Gofryk, F. Ronning, J. Winterlik, G. Fecher, J.-C. Griveau, E. Colineau, C. Felser, J. Thompson *et al.*, Phys. Rev. B **85**, 174505 (2012).
[28] P. Blaha, K. Schwarz, P. Sorantin, and S. Trickey, Comput. Phys. Commun. **59**, 399 (1990).
[29] J. P. Perdew, K. Burke, and M. Ernzerhof, Phys. Rev. Lett. **77**, 3865 (1996).
[30] The plane-wave cutoff parameter RMTKmax was set to 8 and the Brilloun zone (BZ) was sampled by 10000 k points or, in the case of the Pb sublattice calculation, a $3 \times 3 \times 1k$ mesh
[31] F. Tran and P. Blaha, Phys. Rev. Lett. **102**, 226401 (2009).
[32] C. L. Kane and E. J. Mele, Phys. Rev. Lett. **95**, 226801 (2005).
[33] B. Rasche, A. Isaeva, M. Ruck, S. Borisenko, V. Zabolotnyy, B. Büchner, K. Koepernik, C. Ortix, M. Richter, and J. van den Brink, Nat. Mater. **12**, 422 (2013).
[34] P. Dziawa, B. J. Kowalski, K. Dybko, R. Buczko, A. Szczerbakow, M. Szot, E. Łusakowska, T. Balasubramanian, B. M. Wojek, M. H. Berntsen, O. Tjernberg, and T. Story, Nat. Mater. **11**, 1023 (2012).
[35] L. Fu, Phys. Rev. Lett. **106**, 106802 (2011).
[36] T. H. Hsieh, H. Lin, J. Liu, W. Duan, A. Bansil, and L. Fu, Nat. Commun. **3**, 982 (2012).
[37] K. Ishizaka, M. Bahramy, H. Murakawa, M. Sakano, T. Shimojima, T. Sonobe, K. Koizumi, S. Shin, H. Miyahara, A. Kimura *et al.*, Nat. Mater. **10**, 521 (2011).
[38] Z. Zhu, A. Collaudin, B. Fauqué, W. Kang, and K. Behnia, Nat. Phys. **8**, 89 (2011).
[39] C. Fang, M. J. Gilbert, and B. A. Bernevig, arXiv:1308.2424.
[40] F. Di Salvo, G. Hull, Jr., L. Schwartz, J. Voorhoeve, and J. Waszczak, J. Chem. Phys. **59**, 1922 (1973).
[41] M. N. Ali, H. Ji, D. Hirai, M. K. Fuccillo, and R. J. Cava, J. Solid State Chem. **202**, 77 (2013).

MOST WIEDZY Downloaded from mostwiedzy.pl